

Υ suppression in a hadron gas

L. M. Abreu

*Instituto de Física, Universidade Federal da Bahia,
Campus Universitário de Ondina, 40170-115, Bahia, Brazil*

F. S. Navarra

Instituto de Física, Universidade de São Paulo, Rua do Matão 1371, 05508-090 São Paulo, SP, Brazil

M. Nielsen

*Instituto de Física, Universidade de São Paulo, Rua do Matão 1371, 05508-090 São Paulo, SP, Brazil
SLAC Nacional Accelerator Laboratory, Stanford University, Stanford, California 94309, USA*

In this work we study the interactions of bottom mesons which lead to Υ production and absorption in hot hadronic matter. We use effective Lagrangians to calculate the Υ production cross section in processes such as $\bar{B}^{(*)} + B^{(*)} \rightarrow \Upsilon + (\pi, \rho)$ and also the Υ absorption cross section in the corresponding inverse processes. We update and extend previous calculations by Lin and Ko, introducing anomalous interactions. The obtained cross sections are used as input to solve the rate equation which allows us to follow the time evolution of the Υ multiplicity. In contrast to previous conjectures, our results suggest that the interactions in the hadron gas phase strongly reduce the Υ abundance.

I. INTRODUCTION

One of the most interesting predictions of QCD is that strongly interacting matter undergoes a phase transition to a deconfined state at sufficiently high temperatures. The medium composed of quarks and gluons in this deconfined state is referred to as the quark-gluon plasma (QGP) and it has been observed in heavy ion collisions at RHIC [1] and at LHC [2].

Heavy quark bound states are believed to be reliable probes of the quark gluon plasma. In the QGP, once the heavy quarkonium states are formed they are expected to unbind due to the strong interactions with partons in the medium through a QCD Debye screening mechanism [3, 4]. Above a certain temperature, the more weakly bound states, such as $\Upsilon(3S)$, are expected to unbind more completely compared to the more strongly bound states, e.g. $\Upsilon(1S)$. At even higher temperatures, more of the weakly bound states are expected to dissolve. In the experiment, this sequential unbinding (also referred to as melting) of quarkonium states is expected to be observed as a sequential suppression of their yields. The suppression of heavy quarkonium states was accordingly proposed as the smoking-gun signature of the phase transition, and its sequential pattern as a probe of the medium temperature [5].

In the early days most of the attention was devoted to the suppression of charmonium states in collider experiments at SPS and RHIC. However, even after decades of intense efforts, the experimental observations are not yet completely understood. The suppression of $\psi(1S)$ does not increase from SPS to RHIC, or from RHIC to LHC, even though in each change of accelerator the center-of-mass energy is increased by one order of magnitude. The most accepted explanation for this “unsuppression” is that heavy quarks, evolving independently in

the QGP, recombine forming bound states. This process is called recombination or regeneration [5, 6]. It is supposed to take place in the hot plasma and hence to affect mostly the charmonium states produced with transverse momenta typical of the quark-gluon fluid. Indeed, the relative (compared to the scaled pp baseline) reduction of the J/ψ multiplicity measured in AA collisions at low p_T is significantly smaller at LHC energies than at RHIC energies. This is consistent with the regeneration mechanism since the larger charm production cross section at LHC enhances the probability of recombination. The situation changes at high p_T , where the suppression rises as the collision energy increases, revealing that the J/ψ yield is less sensitive to recombination [7–9].

While charmonium states have been extensively studied as QGP probes, bottomonium states were not explored so much, even though the $b\bar{b}$ family of states provides experimentally more robust and theoretically cleaner probes. Moreover, bottomonium states are regarded as better probes because recombination effects are believed to be much less significant than in the charmonium case. Although the recombination effect is expected to increase for bottomonia from RHIC to LHC energies, it is predicted to remain small [10–15].

From the experimental side, the CMS detector has excellent capabilities for muon detection and provides measurements of the Υ family which enable the accurate analysis of bottomonium [16] production. For this reason, the main interest may be shifted to the suppression of bottomonium states at LHC energies. The first indication of Υ suppression in heavy ion collisions was reported by CMS in 2011 [17]. Later it was also observed by the STAR Collaboration at RHIC [18]. The $\Upsilon(2S)$ and $\Upsilon(3S)$ resonances in PbPb collisions were seen to be more strongly suppressed than the $\Upsilon(1S)$ (compared with the pp result), showing the expected sequential suppression pattern [16].

The most recent data on prompt J/ψ [19] and Υ [16, 20–22] suppression in the most central Pb Pb collisions at small rapidities and small p_T , show that:

$$R_{AA}(J/\psi) \simeq 0.28 \pm 0.03 \quad (1)$$

and

$$R_{AA}(\Upsilon(1S)) \simeq 0.38 \pm 0.05 \quad (2)$$

These factors are very weakly dependent on the collision energy \sqrt{s}_{NN} . Although they are close to each other, they may be the result of a quite different dynamics.

After the QGP cooling and hadronization there is a hadron gas (HG) phase. Apart from being a reasonable assumption, the existence of this phase seems to be necessary to correctly reproduce [23] the multiplicities of K^* and ρ measured by the ALICE Collaboration [24–26]. Heavy quarkonium is produced at the beginning of the heavy ion collision. Then it may be destroyed and regenerated both in the quark gluon plasma and in the subsequent hadron gas. The observed Υ suppression has been explained mostly with models which take into account only what happens during the QGP phase. In this work we address the contribution of the hadron gas phase to the Υ production and absorption.

In the literature, there is a large number of works on quarkonium interactions with light mesons in a hot hadron gas using different approaches (for a short and recent compilation of references on charmonium interactions, see [27]). Many of these works investigate the J/ψ -light meson reactions based on effective hadron Lagrangians [27–30]. After a long series of works, different groups found a similar value of the $J/\psi - \pi$ cross section, which is close to the value obtained with QCD sum rules [31]. In [27], we have used all the known charmonium-light hadron absorption cross sections (together with the inverse interactions in which charmonium is produced) as input to solve the rate equation which governs the time evolution of J/ψ abundance in a hadron gas. The effective Lagrangian approach will be employed also to the bottomonium in the next sections.

In contrast to the J/ψ case, the number of studies about the Υ interactions with light hadrons is much smaller. In fact, to the best of our knowledge, the paper by Lin and Ko, Ref. [32], is the only one to give an estimate of the cross sections for scattering of Υ by pions and ρ mesons in a hot hadron gas. In that work the authors used a hadronic Lagrangian based on the $SU(5)$ flavor symmetry. Including form factors with a cutoff parameter of 1 or 2 GeV at the interaction vertices, they found that the values of $\sigma_{\pi\Upsilon}$ and $\sigma_{\rho\Upsilon}$ are about 8 mb and 1 mb, respectively. However, due to the large kinematic threshold, their thermal averages at a temperature of 150 MeV are both only about 0.2 mb. They then conclude speculating that the absorption of directly produced Υ by comoving hadrons is unlikely to be important.

In view of the recent theoretical and experimental progress on Υ physics, we believe that it is time to update and extend the calculation of Ref. [32]. In the

present work we will contribute to this subject extending the analysis performed in Ref. [27] to the bottomonia sector: we investigate the interactions of Υ with the surrounding hadronic medium composed of the lightest pseudoscalar meson (π) and the lightest vector meson (ρ). We calculate the cross sections for processes such as $\bar{B}^{(*)} + B^{(*)} \rightarrow \Upsilon + (\pi, \rho)$ scattering and their inverses, within the effective hadron Lagrangian framework. We improve the previous calculation introducing anomalous interactions. The obtained cross sections are used as input to solve the rate equation which allows us to follow the time evolution of the Υ multiplicity.

The importance of the anomalous vertices has been earlier mentioned in different contexts. For example, in Ref. [29] the J/ψ absorption cross sections by pions and ρ mesons were evaluated for several processes producing D and D^* mesons in the final state. The authors found that the $J/\psi\pi \rightarrow D^*\bar{D}$ cross section obtained with the exchange of a D^* meson in the t-channel, which involves the anomalous $D^*D^*\pi$ coupling, was around 80 times bigger than the one obtained with a D meson exchange in the t-channel. In Ref. [33] the authors studied the radiative decay modes of the $f_0(980)$ and $a_0(980)$ resonances, finding that the diagrams involving anomalous couplings were quite important for most of the decays. More recently, in Refs. [34, 35] it was shown that the inclusion of anomalous interactions produces significant changes in the $X(3872)\pi$ cross section.

This work is organized as follows. In Section II we present an overview of the effective Lagrangian formalism and calculate the cross section for Υ production and absorption. The results obtained for the thermally averaged cross sections are exhibited and discussed in Section III. After that, Section IV is dedicated to the analysis of Υ abundance in heavy ion collisions. Finally, in Section V we summarize the results and conclusions.

II. INTERACTIONS BETWEEN Υ AND LIGHT MESONS

A. Effective Lagrangian Formalism

In the present study the reactions involving the Υ production and absorption will be analyzed in the effective field theory approach. Accordingly, we follow Refs. [27–29] and employ the couplings between light- and heavy-meson fields within the framework of an $SU(4)$ effective formalism, in which the vector mesons are identified as the gauge bosons, and the interaction Lagrangians are given by

$$\begin{aligned} \mathcal{L}_{PPV} &= -ig_{PPV}\langle V^\mu [P, \partial_\mu P] \rangle, \\ \mathcal{L}_{VVV} &= ig_{VVV}\langle \partial_\mu V_\nu [V^\mu, V^\nu] \rangle, \\ \mathcal{L}_{PPVV} &= g_{PPVV}\langle PV^\mu [V_\mu, P] \rangle, \\ \mathcal{L}_{VVVV} &= g_{VVVV}\langle V^\mu V^\nu [V_\mu, V_\nu] \rangle, \end{aligned} \quad (3)$$

where the indices PPV and VVV , $PPVV$ and $VVVV$ denote the type of vertex incorporating pseudoscalar (P) and vector (V) meson fields in the couplings [28, 29] and g_{PPV} , g_{VVV} , g_{PPVV} and g_{VVVV} are the respective coupling constants. The symbol $\langle \dots \rangle$ stands for the trace over $SU(4)$ -matrices. V_μ represents a $SU(4)$ matrix, which is parametrized by 16 vector-meson fields including the 15-plet and singlet of $SU(4)$,

$$V_\mu = \begin{pmatrix} \frac{\omega}{\sqrt{2}} + \frac{\rho^0}{\sqrt{2}} & \rho^+ & K^{*+} & \bar{B}^{*0} \\ \rho^- & \frac{\omega}{\sqrt{2}} - \frac{\rho^0}{\sqrt{2}} & K^{*0} & B^{*-} \\ K^{*-} & \bar{K}^{*0} & \phi & B_s^{*-} \\ B^{*0} & B^{*+} & B_s^{*+} & \Upsilon \end{pmatrix}_\mu; \quad (4)$$

P is a matrix containing the 15-plet of the pseudoscalar meson fields, written in the physical basis in which η , η' mixing is taken into account,

$$P = \begin{pmatrix} \frac{\eta}{\sqrt{3}} + \frac{\eta'}{\sqrt{6}} + \frac{\pi^0}{\sqrt{2}} & \pi^+ & K^+ & \bar{B}^0 \\ \pi^- & \frac{\eta}{\sqrt{3}} + \frac{\eta'}{\sqrt{6}} - \frac{\pi^0}{\sqrt{2}} & K^0 & B^- \\ K^{*-} & \bar{K}^{*0} & -\frac{\eta}{\sqrt{3}} + \sqrt{\frac{2}{3}}\eta' & B_s^- \\ B^0 & B^+ & B_s^+ & \eta_b \end{pmatrix}.$$

We also consider anomalous parity interactions in addition to the couplings given above. The anomalous parity interactions can be described in terms of the gauged

Wess-Zumino action [29], and are written as

$$\begin{aligned} \mathcal{L}_{PVV} &= -g_{PVV}\varepsilon^{\mu\nu\alpha\beta}\langle\partial_\mu V_\nu\partial_\alpha V_\beta P\rangle, \\ \mathcal{L}_{PPPV} &= -ig_{PPPV}\varepsilon^{\mu\nu\alpha\beta}\langle V_\mu(\partial_\nu P)(\partial_\alpha P)(\partial_\beta P)\rangle, \\ \mathcal{L}_{PVVV} &= ig_{PVVV}\varepsilon^{\mu\nu\alpha\beta}\left[\langle V_\mu V_\nu V_\alpha\partial_\beta P\rangle \right. \\ &\quad \left. + \frac{1}{3}\langle V_\mu(\partial_\nu V_\alpha)V_\beta P\rangle\right]. \end{aligned} \quad (5)$$

The g_{PVV} , g_{PPPV} , g_{PVVV} are the coupling constants of the PVV , $PPPV$ and $PVVV$ vertices, respectively [27–29].

The effective Lagrangians given in Eqs. (3) and (5) allow us to study the following $\varphi\Upsilon$ absorption processes

$$\begin{aligned} (1) \quad &\varphi\Upsilon \rightarrow \bar{B}B, \\ (2) \quad &\varphi\Upsilon \rightarrow \bar{B}^*B, \\ (3) \quad &\varphi\Upsilon \rightarrow \bar{B}^*B^*, \end{aligned} \quad (6)$$

where in the initial states φ stand for pions and ρ mesons. The process $\varphi\Upsilon \rightarrow \bar{B}B^*$ has the same cross section as the process (2) in Eq. (6). In the present approach, the diagrams considered to compute the amplitudes of the processes above are of two types: one-meson exchange and contact graphs. They are shown in Fig. 1 and 2 for those with pions and ρ , respectively.

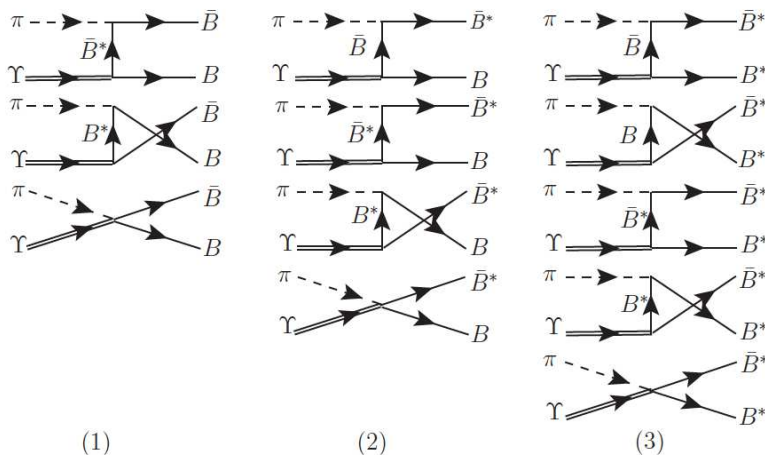


FIG. 1. Diagrams contributing to the processes: (1) $\pi\Upsilon \rightarrow \bar{B}B$, (2) $\pi\Upsilon \rightarrow \bar{B}^*B$, and (3) $\pi\Upsilon \rightarrow \bar{B}^*B^*$.

We define the invariant amplitudes for the processes

(1)-(3) in Eq. (6) involving $\varphi = \pi$ meson as

$$\begin{aligned} \mathcal{M}_1^{(\pi)} &= \sum_i \mathcal{M}_{1i}^{(\pi)\mu} \epsilon_\mu(p_1), \\ \mathcal{M}_2^{(\pi)} &= \sum_i \mathcal{M}_{2i}^{(\pi)\mu\nu} \epsilon_\mu(p_1) \epsilon_\nu^*(p_3), \\ \mathcal{M}_3^{(\pi)} &= \sum_i \mathcal{M}_{3i}^{(\pi)\mu\nu\lambda} \epsilon_\mu(p_1) \epsilon_\nu^*(p_3) \epsilon_\lambda^*(p_4), \end{aligned} \quad (7)$$

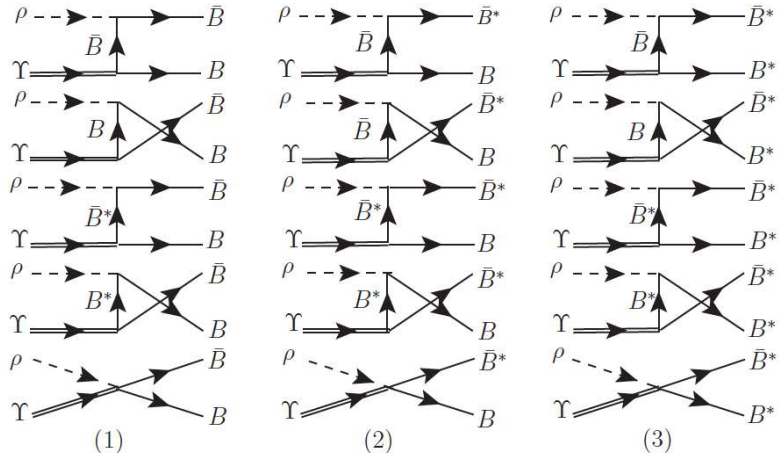


FIG. 2. Diagrams contributing to the processes: (1) $\rho\Upsilon \rightarrow \bar{B}B$, (2) $\rho\Upsilon \rightarrow \bar{B}^*B$, and (3) $\rho\Upsilon \rightarrow \bar{B}^*B^*$.

while for the ones involving $\varphi = \rho$ meson we have

$$\begin{aligned}\mathcal{M}_1^{(\rho)} &= \sum_i \mathcal{M}_{1i}^{(\rho)\mu\nu} \epsilon_\mu(p_1) \epsilon_\nu(p_2), \\ \mathcal{M}_2^{(\rho)} &= \sum_i \mathcal{M}_{2i}^{(\rho)\mu\nu\lambda} \epsilon_\mu(p_1) \epsilon_\nu(p_2) \epsilon_\lambda^*(p_3), \\ \mathcal{M}_3^{(\rho)} &= \sum_i \mathcal{M}_{3i}^{(\rho)\mu\nu\lambda\delta} \epsilon_\mu(p_1) \epsilon_\nu(p_2) \epsilon_\lambda^*(p_3) \epsilon_\delta^*(p_4). \quad (8)\end{aligned}$$

In the above equations, the sum over i represents the sum over all diagrams contributing to the respective amplitude; p_j denotes the momentum of particle j , with particles 1 and 2 standing for initial state mesons, and particles 3 and 4 for final state mesons; $\epsilon_\mu(p_j)$ is the polarization vector related to the respective vector particle j . The specific expressions of amplitudes $\mathcal{M}_i^{(\pi)}$ and $\mathcal{M}_i^{(\rho)}$ in the present case are analogous to the ones given in Ref. [29] involving $\varphi J/\psi \rightarrow D^{(*)} \bar{D}^{(*)}$. So, we will not reproduce here the explicit expressions of the invariant amplitudes. These expressions can be found in Ref. [29], taking into account the replacement of masses and coupling constants labeled with charmed mesons and J/ψ by similar quantities labeled with bottomed mesons and Υ , respectively.

The isospin-spin-averaged cross section for the processes in Eq. (6) is defined in the center of mass (CM) frame as

$$\sigma_r^{(\varphi)}(s) = \frac{1}{64\pi^2 s} \frac{|\vec{p}_f|}{|\vec{p}_i|} \int d\Omega \overline{\sum_{S,I}} |\mathcal{M}_r^{(\varphi)}(s, \theta)|^2, \quad (9)$$

where $r = 1, 2, 3$ labels $\varphi - \Upsilon$ absorption processes according to Eqs. (7) and (8); \sqrt{s} is the CM energy; $|\vec{p}_i|$ and $|\vec{p}_f|$ denote the three-momenta of initial and final particles in the CM frame, respectively; the symbol $\overline{\sum_{S,I}}$ represents the sum over the spins and isospins of the particles in the initial and final state, weighted by the isospin and spin degeneracy factors of the two particles forming the initial

TABLE I. Values of coupling constants [29, 32].

Coupling constant	Value
$g_{B^*B\pi}$	24.9
$g_{\Upsilon BB}$	13.3
$g_{\Upsilon B^*B^*}$	13.3
$g_{BB\rho}$	2.52
$g_{B^*B^*\rho}$	2.52
$g_{\Upsilon B^*B\pi}$	165.6
$g_{\Upsilon BB\rho}$	67.03
$g_{\Upsilon B^*B^*\rho}$	33.5
$g_{B^*B^*\pi}$	9.39 GeV ⁻¹
$g_{\Upsilon B^*B}$	2.51 GeV ⁻¹
$g_{B^*B\rho}$	1.84 GeV ⁻¹
$g_{\Upsilon BB\pi}$	44.8 GeV ⁻³
$g_{\Upsilon B^*B^*\pi}$	31.25 GeV ⁻¹
$h_{\Upsilon B^*B^*\pi}$	31.25 GeV ⁻¹
$g_{\Upsilon B^*B\rho}$	6.33 GeV ⁻¹
$h_{\Upsilon B^*B\rho}$	6.33 GeV ⁻¹

state for the reaction r , i.e.

$$\overline{\sum_{S,I}} |\mathcal{M}_r|^2 = \frac{1}{g_1 g_2} \sum_{S,I} |\mathcal{M}_r|^2, \quad (10)$$

with $g_1 = (2I_{1i,r} + 1)(2S_{1i,r} + 1)$, $g_2 = (2I_{2i,r} + 1)(2S_{2i,r} + 1)$ being the degeneracy factors of the initial particles 1 and 2.

We have employed in the computations of the present work the isospin-averaged masses: $m_\pi = 137.3$ MeV, $m_\rho = 775.2$ MeV, $m_B = 5279.4$ MeV, $m_{B^*} = 5324.7$ MeV, $m_\Upsilon = 9460.3$ MeV. The values of coupling constants appearing in the expressions of the amplitudes $\mathcal{M}^{(\pi)}$ and $\mathcal{M}^{(\rho)}$ are given in Table I [29, 32].

We have also included form factors in the vertices when

evaluating the cross sections, defined as [36–38]:

$$F_3 = \left(\frac{n\Lambda^4}{n\Lambda^4 + (p^2 - m_{ex}^2)^2} \right)^n, \\ F_4 = \left(\frac{n\Lambda^4}{n\Lambda^4 + [(p_1 + p_2)^2 - (m_3 + m_4)^2]} \right)^n, \quad (11)$$

where F_3 and F_4 are the form factor for the three-point and four-point vertices, respectively; p is the four-momentum of the exchanged particle of mass m_{ex} for a vertex involving a t - or u -channel meson exchange; m_3 and m_4 are the final state meson masses. The cutoff Λ and n parameters are chosen to be $\Lambda = 5.0$ GeV and $n \rightarrow \infty$ for all vertices, which gives Gaussian form factors with width 25.0 GeV².

B. Υ production and absorption cross sections

On the top panel of Fig. 3 the $\pi\Upsilon$ absorption cross sections for the $\pi\Upsilon \rightarrow \bar{B}B, \bar{B}^*B$ and \bar{B}^*B^* reactions are plotted as a function of the CM energy \sqrt{s} . We see that the cross sections can be considered to be approximately of the same order of magnitude in the range 10.6 GeV $\leq \sqrt{s} \leq 11.8$ GeV, differing by about a factor 1.5-3. The magnitude of the reaction $\pi\Upsilon \rightarrow \bar{B}^*B$ is in agreement with previous calculations reported in Ref. [32], which is based in $SU(5)$ symmetry, using different form factors, cutoffs and coupling constants and without anomalous terms. The authors of Ref. [32] did not include some of the processes with final states $\bar{B}B$ and \bar{B}^*B^* .

The cross sections of the processes $\rho\Upsilon \rightarrow \bar{B}B, \bar{B}^*B$ and \bar{B}^*B^* are plotted as a function of \sqrt{s} on the bottom panel of Fig. 3. In this case the cross section for $\rho\Upsilon \rightarrow \bar{B}^*B^*$ is larger than the others by about one order of magnitude. As expected, the $\rho - \Upsilon$ reactions have smaller cross sections than those initiated by pions. The findings above are also in relative agreement with the previous calculations reported in Ref. [32], although only the processes which end with $\bar{B}B$ and \bar{B}^*B^* have been considered in [32]. Again, we believe that the differences are due to different choices in the form factors and cutoff values, and the absence of anomalous parity interactions.

For completeness, we now calculate the cross sections of the inverse processes, which can be obtained from the direct processes through the use of detailed balance (see for example Eq. (48) of the last article of Ref. [28]). In the top (bottom) panel of Fig. 4 the $\pi(\rho)\Upsilon$ production cross sections for the $\bar{B}B \rightarrow \pi(\rho)\Upsilon, \bar{B}B^* \rightarrow \pi(\rho)\Upsilon$ and $\bar{B}^*B^* \rightarrow \pi(\rho)\Upsilon$ reactions are plotted as a function of the CM energy \sqrt{s} .

From these Figures we can see that: i) processes which start or end with $\pi\Upsilon$ have larger cross sections. ii) Excluding the low energy region (which will be much less relevant for phenomenology), the Υ production and absorption cross sections are close to each other in almost all channels. Therefore, taking into account that the Υ absorption and production cross sections have comparable magnitudes, the computation of thermally averaged

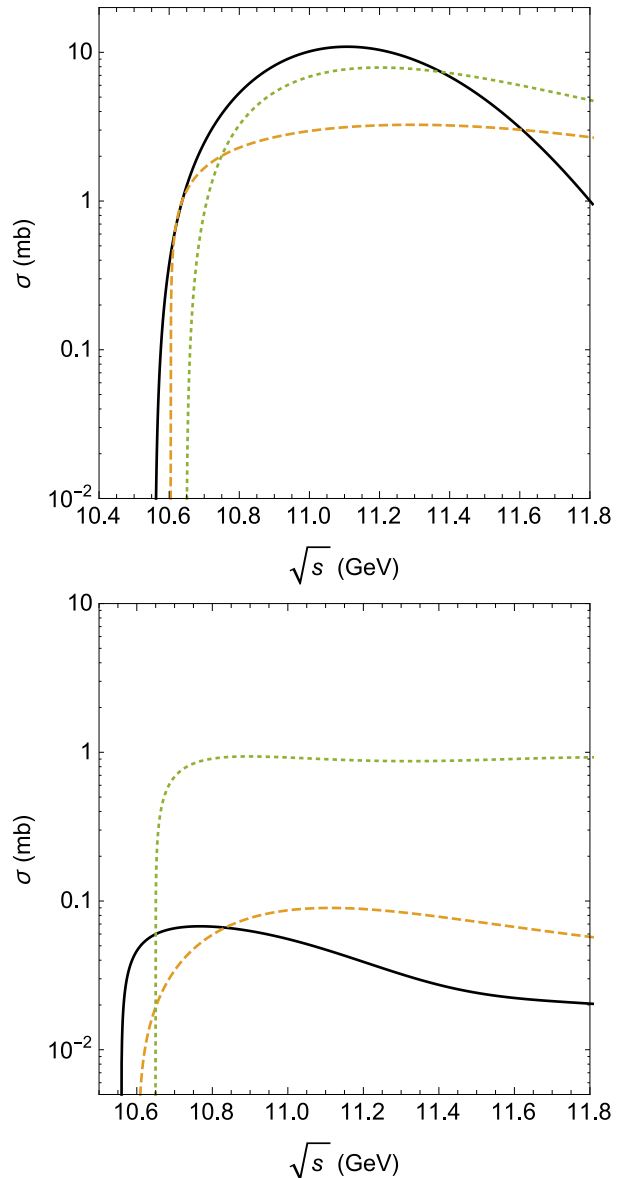


FIG. 3. Υ absorption cross sections in different processes as a function of the CM energy \sqrt{s} . Top panel: $\pi\Upsilon$ in the initial state. Bottom panel: $\rho\Upsilon$ in the initial state. Solid, dashed and dotted lines represent the $\pi(\rho)\Upsilon \rightarrow \bar{B}B, \pi(\rho)\Upsilon \rightarrow \bar{B}^*B$ and $\pi(\rho)\Upsilon \rightarrow \bar{B}^*B^*$ reactions, respectively.

cross sections is an essential step to determine the final abundance of Υ 's. This will be done in next Section.

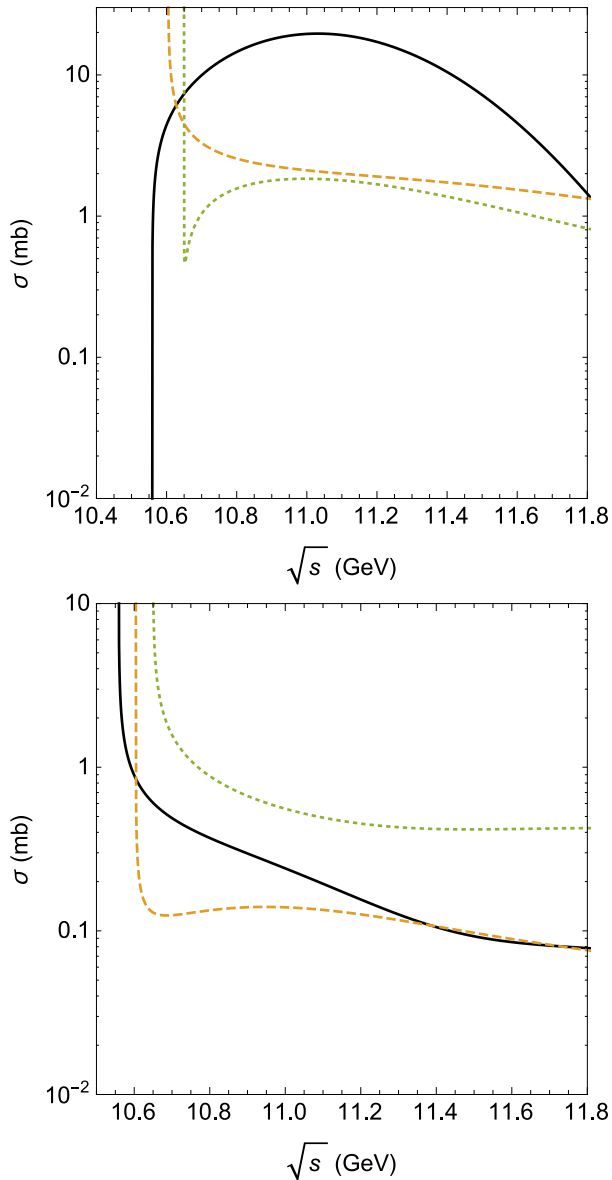


FIG. 4. Υ production cross sections in different processes as a function of the CM energy \sqrt{s} . Top panel: $\pi\Upsilon$ in the final state. Bottom panel: $\rho\Upsilon$ in the final state. Solid, dashed and dotted lines represent the $\bar{B}B \rightarrow \pi(\rho)\Upsilon$, $\bar{B}^*B \rightarrow \pi(\rho)\Upsilon$ and $\bar{B}^*B^* \rightarrow \pi(\rho)\Upsilon$ reactions, respectively.

III. THERMALLY AVERAGED CROSS SECTIONS

The thermally averaged cross section for a given process $ab \rightarrow cd$ is defined as [34, 39–41]

$$\begin{aligned} \langle \sigma_{ab \rightarrow cd} v_{ab} \rangle &= \frac{\int d^3\mathbf{p}_a d^3\mathbf{p}_b f_a(\mathbf{p}_a) f_b(\mathbf{p}_b) \sigma_{ab \rightarrow cd} v_{ab}}{\int d^3\mathbf{p}_a d^3\mathbf{p}_b f_a(\mathbf{p}_a) f_b(\mathbf{p}_b)} \\ &= \frac{1}{4\alpha_a^2 K_2(\alpha_a) \alpha_b^2 K_2(\alpha_b)} \\ &\quad \times \int_{z_0}^{\infty} dz K_1(z) \sigma(s = z^2 T^2) \\ &\quad \times [z^2 - (\alpha_a + \alpha_b)^2] [z^2 - (\alpha_a - \alpha_b)^2], \end{aligned} \quad (12)$$

where v_{ab} represents the relative velocity of initial two interacting particles a and b ; the function $f_i(\mathbf{p}_i)$ is the Bose-Einstein distribution (of particles of species i), which depends on the temperature T ; $\alpha_i = m_i/T$, $z_0 = \max(\alpha_a + \alpha_b, \alpha_c + \alpha_d)$, and K_1 and K_2 the modified Bessel functions of second kind.

In Fig. 5 we plot the thermally averaged cross sections for $\pi\Upsilon$ absorption (upper panel) and production (lower panel) via the processes discussed in previous section. We can see that reactions which start or end with $\bar{B}B$ have greater magnitudes. But the main point here is that the production reactions have larger cross sections than the absorption ones.

In Fig. 6 we plot the thermally averaged cross sections for the $\rho\Upsilon$ absorption and production. As before, in general the production reactions have larger cross sections than the corresponding inverse reactions. The absorption and production reactions which start or end with \bar{B}^*B and \bar{B}^*B^* are comparable at high temperatures, while the production from the $\bar{B}B$ initial state is stronger than the absorption with the $\bar{B}B$ final state.

IV. TIME EVOLUTION OF THE J/ψ ABUNDANCE

The present study will be completed by addressing the time evolution of the Υ abundance in hadronic matter, using the thermally averaged cross sections estimated in the previous section. We shall make use of the evolution equation for the abundances of particles included in processes discussed above. The momentum-integrated evolution equation has the form [34, 40–45]:

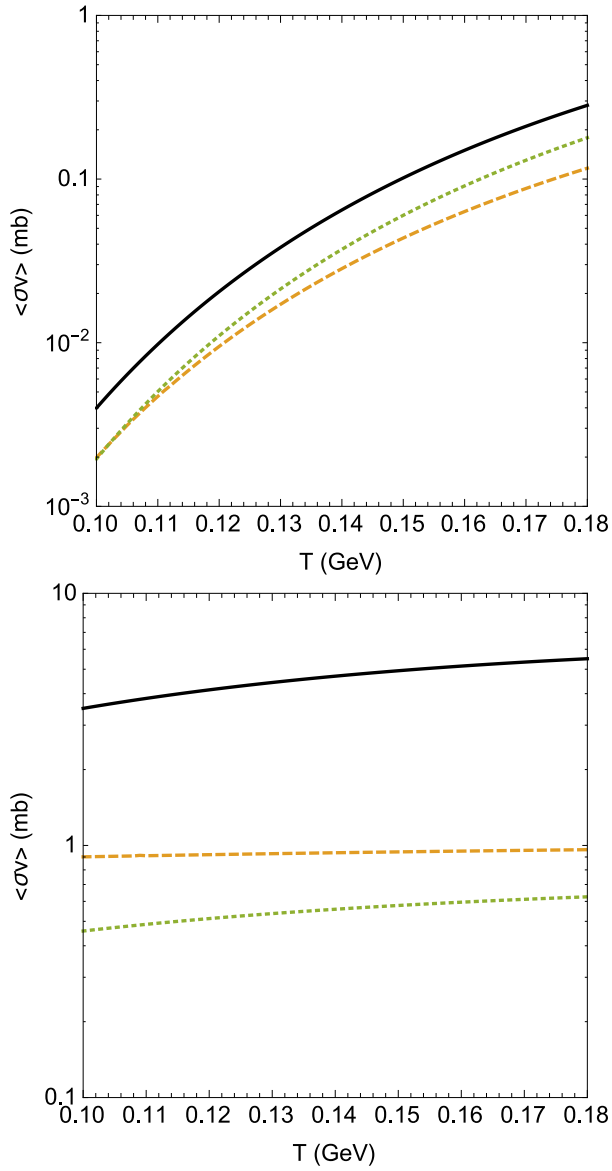


FIG. 5. Thermally averaged cross sections for $\pi\Upsilon$ absorption and production as a function of the temperature. Top panel: $\pi\Upsilon$ in the initial state. Bottom panel: $\pi\Upsilon$ in the final state. Solid, dashed and dotted lines represent the reactions with $\bar{B}B$, \bar{B}^*B and \bar{B}^*B^* , respectively, in final or initial state.

$$\begin{aligned} \frac{dN_\Upsilon(\tau)}{d\tau} = & \sum_{\varphi=\pi,\rho} \left[\langle\sigma_{\bar{B}B\rightarrow\varphi\Upsilon} v_{\bar{B}B}\rangle n_{\bar{B}}(\tau) N_B(\tau) \right. \\ & - \langle\sigma_{\varphi\Upsilon\rightarrow\bar{B}B} v_{\varphi\Upsilon}\rangle n_\varphi(\tau) N_\Upsilon(\tau) \\ & + \langle\sigma_{\bar{B}^*B^*\rightarrow\varphi\Upsilon} v_{\bar{B}^*B^*}\rangle n_{\bar{B}^*}(\tau) N_{B^*}(\tau) \\ & - \langle\sigma_{\varphi\Upsilon\rightarrow\bar{B}^*B^*} v_{\varphi\Upsilon}\rangle n_\varphi(\tau) N_\Upsilon(\tau) \\ & + \langle\sigma_{B^*B\rightarrow\varphi\Upsilon} v_{B^*B}\rangle n_{B^*}(\tau) N_B(\tau) \\ & - \langle\sigma_{\varphi\Upsilon\rightarrow\bar{B}^*B} v_{\varphi\Upsilon}\rangle n_\varphi(\tau) N_\Upsilon(\tau) \\ & + \langle\sigma_{\bar{B}B^*\rightarrow\varphi\Upsilon} v_{\bar{B}B^*}\rangle n_{\bar{B}}(\tau) N_{B^*}(\tau) \\ & \left. - \langle\sigma_{\varphi\Upsilon\rightarrow\bar{B}B^*} v_{\varphi\Upsilon}\rangle n_\varphi(\tau) N_\Upsilon(\tau) \right], \quad (13) \end{aligned}$$

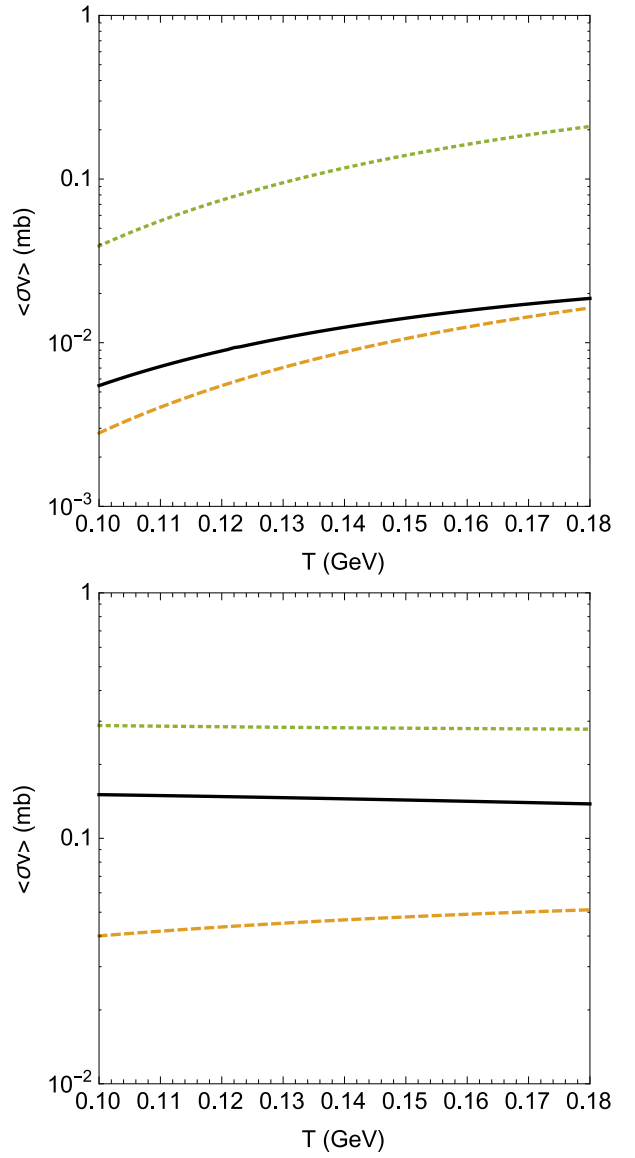


FIG. 6. Thermally averaged cross sections for $\rho\Upsilon$ absorption and production as a function of the temperature. Top panel: $\rho\Upsilon$ in the initial state. Bottom panel: $\rho\Upsilon$ in the final state. Solid, dashed and dotted lines represent the reactions with $\bar{B}B$, \bar{B}^*B and \bar{B}^*B^* , respectively, in final or initial state.

where $n_i(\tau)$ are $N_i(\tau)$ denote the density and the abundances of π , ρ and bottom mesons in hadronic matter at proper time τ . From Eq. (13) we notice that the Υ abundance at a proper time τ depends on the $\varphi\Upsilon$ dissociation rate as well as on the $\varphi\Upsilon$ production rate. We will assume that π , ρ , B and B^* are in equilibrium. Therefore the density $n_i(\tau)$ can be written as [34, 40–43]

$$n_i(\tau) \approx \frac{1}{2\pi^2} \gamma_i g_i m_i^2 T(\tau) K_2 \left(\frac{m_i}{T(\tau)} \right), \quad (14)$$

where γ_i and g_i are the fugacity factor and the degeneracy factor of the relevant particle, respectively. The multiplicity $N_i(\tau)$ is obtained by multiplying the density

$n_i(\tau)$ by the volume $V(\tau)$. The time dependence is introduced through the temperature, $T(\tau)$, and volume, $V(\tau)$, profiles, appropriate to model the dynamics of relativistic heavy ion collisions after the end of the quark-gluon plasma phase. The hydrodynamical expansion and cooling of the hadron gas are described as in Refs. [34, 40–45], which are based on the boost invariant Bjorken picture with an accelerated transverse expansion:

$$\begin{aligned} T(\tau) &= T_C - (T_H - T_F) \left(\frac{\tau - \tau_H}{\tau_F - \tau_H} \right)^{\frac{4}{5}}, \\ V(\tau) &= \pi \left[R_C + v_C (\tau - \tau_C) + \frac{a_C}{2} (\tau - \tau_C)^2 \right]^2 \tau c, \end{aligned} \quad (15)$$

where R_C and τ_C denote the final transverse and longitudinal sizes of the quark-gluon plasma; v_C and a_C are its transverse flow velocity and transverse acceleration at τ_C ; $T_C = 175$ MeV is the critical temperature for the quark-gluon plasma to hadronic matter transition; $T_H = T_C = 175$ MeV is the temperature of the hadronic matter at the end of the mixed phase, occurring at the time τ_H ; and the freeze-out temperature, $T_F = 125$ MeV, leads to a freeze-out time τ_F .

In the present approach we assume that the total number of bottom quarks in bottom hadrons is conserved during the processes. This number can be calculated with perturbative QCD and yields the bottom quark fugacity factor γ_b in Eq. (14) [34, 40–43]. The total number of pions and ρ mesons at freeze-out was taken from Refs. [34, 44, 45].

The evolution of Υ multiplicity is analyzed in two scenarios: with the hadron gas formed in central $Au - Au$ collisions at $\sqrt{s_{NN}} = 200$ GeV at RHIC and central $Pb - Pb$ collisions at $\sqrt{s_{NN}} = 5$ TeV at the LHC. The parameters which we need as input in Eqs. (15) are listed in Ref. [42], and are reproduced in Table II for convenience. Notice that the estimate of the Υ yield at the end of the mixed phase, given in the last column of Table II, is done in the context of the statistical model, in which hadrons are in thermal and chemical equilibrium when they are produced. Therefore, at RHIC the Υ multiplicity at τ_H is

$$\begin{aligned} N_\Upsilon &\approx \frac{1}{2\pi^2} \gamma_b^2 g_\Upsilon m_\Upsilon^2 T_H K_2 \left(\frac{m_\Upsilon}{T_H} \right) V(\tau_H) \\ &\approx 1.705 \times 10^6. \end{aligned} \quad (16)$$

A similar calculation for the case of LHC gives $N_\Upsilon \approx 0.00106$.

TABLE II. Parameters used in the parametrization of the hydrodynamical expansion, given by Eqs. (15).

	$\sqrt{s_{NN}}$ (TeV)	v_C (c)	a_C (c ² /fm)	R_C (fm)	τ_C (fm/c)	τ_H (fm/c)	τ_F (fm/c)	γ_b	N_Υ
RHIC	0.2	0.4	0.02	8	5	7.5	17.3	2.2×10^6	1.705×10^6
LHC	5	0.6	0.044	13.11	5	7.5	20.7	3.3×10^7	0.00106

The time evolution of the Υ abundance is plotted in Fig. 7 as a function of the proper time, for the two types of collisions discussed above: at RHIC (on the upper panel) and at the LHC (on the lower panel).

The behavior of the Υ multiplicity observed in Fig. 7 is not difficult to understand. Due to the assumption that the hadronic stage at LHC is longer compared to that at RHIC, more bottomonium states are lost in the hadronic medium at LHC. Also, it can be noticed, from Eq. (13), that the evolution of the Υ multiplicity depends on the production and absorption cross sections and also on the abundances of the other mesons. Although the production cross sections are greater than the absorption ones, which would enhance the Υ yield, the relative meson multiplicities lead to its reduction, since there are much more light mesons (especially pions) in the hadron gas to collide and destroy the bottomonium states than $B^{(*)}$'s and $\bar{B}^{(*)}$'s to interact and create them. Besides, from the solid and dotted lines in Fig. 7 we can infer

that the role of the ρ mesons in the gas is not relevant when compared to that of the pions. This comes from a cancellation between the terms associated to the production and absorption reactions: the different magnitudes of production and absorption processes are compensated by the relative multiplicities.

The results shown in Fig. 7 suggest a decrease of the Υ yield of almost $\simeq 66$ % at RHIC and $\simeq 70$ % at the LHC. These numbers are compatible with (2). Taken literally, they would suggest that all the suppression comes from the hadron gas phase. However we are not yet in the position of sustaining this strong statement. Before that, there is a number of points to be discussed. First the interactions in the reactions are naturally dependent on the effective formalism considered, which determines the magnitudes of the cross sections. A change in the magnitude of the production reactions will modify those of the absorption in the same proportion. This will lead to an overall multiplicative factor in the right hand side

of rate equation, Eq. (13), modifying the curves in Fig. 7. Besides, our results are strongly dependent on the form factors and cutoff values: different choices would modify the slope of the curves in Fig. 7. Furthermore, the relevance of the parametrization of the hydrodynamical expansion exhibited in Eq. (15) can not be underestimated. Different parameters can make the system cool faster or slower and accordingly change the multiplicities of the distinct particles.

Notwithstanding the points raised above, we stress the main result of this work: a reduction of the number of Υ 's in the hadron gas, which seems to be larger than in the case of J/ψ reported in Ref. [27]. Before closing this section, we show in Fig. 8 a comparison between the Υ and J/ψ multiplicities as a function of the proper time. The latter one was already published in [27]. For the sake of comparison we have rescaled them to the unity at the initial time. The J/ψ suppression is only of $\simeq 25\%$, whereas it is of $\simeq 70\%$ in the case of the Υ .

V. CONCLUDING REMARKS

In this work we have analyzed the hadronic effects on the Υ abundance in heavy ion collisions. Effective Lagrangians have been used to calculate the cross sections for the Υ -production processes $\bar{B}^{(*)} + B^{(*)} \rightarrow \Upsilon + (\pi, \rho)$, and also for the corresponding inverse processes associated to the Υ absorption. We have also computed the thermally averaged cross sections for the dissociation and production reactions. Finally, we have employed the thermally averaged cross sections as inputs in the rate equation and have determined the time evolution of the Υ abundance in a hadron gas.

Examining the existing literature on cross section calculations, the present work has introduced the following improvements: inclusion of reactions which start or end with $\bar{B}B$ and \bar{B}^*B^* in the case of the pion- Υ scattering, and \bar{B}^*B in that involving ρ meson; inclusion of the anomalous parity interactions processes in the effective Lagrangian approach.

Our results suggest that the interactions between Υ and light mesons reduce the Υ abundance at the end of the quark gluon plasma phase by $\simeq 70\%$, which is more than in the case of the J/ψ reported in Ref. [27].

In conclusion, despite the fact that there are points to be improved to obtain a more realist description of the HIC phenomenology, we believe that our findings are important for the physics of both the quark gluon plasma and hadronic phases. Our result should encourage further studies of the Υ suppression in the hadron gas phase of relativistic heavy ion collisions.

ACKNOWLEDGMENTS

The authors would like to thank the Brazilian funding agencies CNPq (contracts 310759/2016-1, 311524/2016-

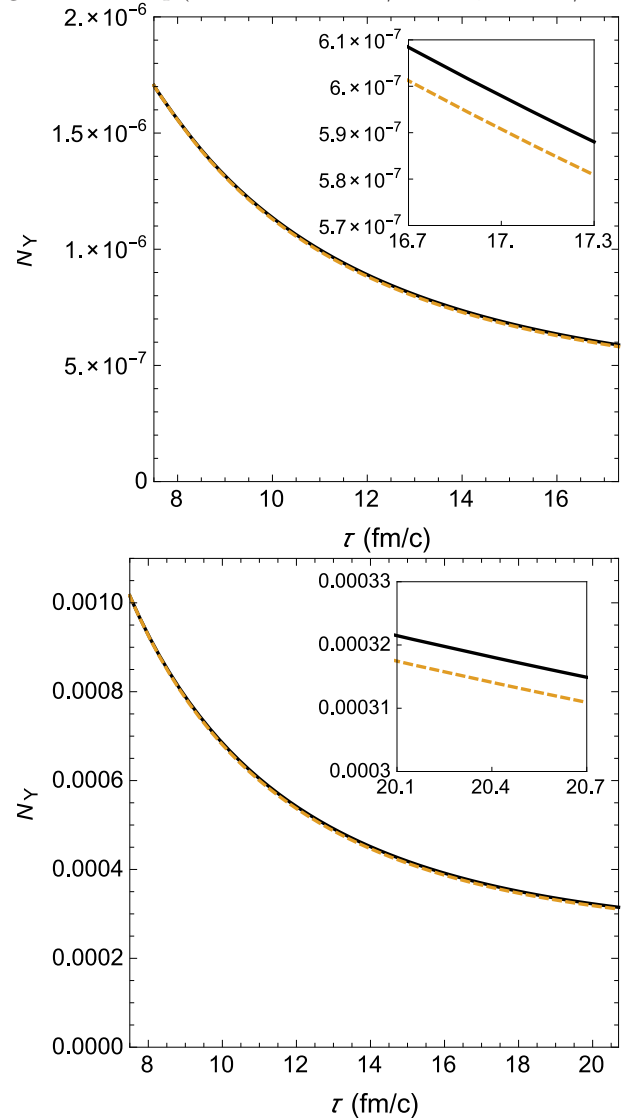


FIG. 7. Top: Time evolution of Υ abundance as a function of the proper time in central Au-Au collisions at $\sqrt{s_{NN}} = 200$ GeV. Solid and dashed lines represent the situations with only $\pi - \Upsilon$ interactions and also adding the $\rho - \Upsilon$, respectively. Bottom: the same as on the top for LHC conditions.

8, 308088/2017-4 and 400546/2016-7), FAPESP (contract 17/07278-5) FAPESB (contract INT0007/2016) for financial support.

[1] J. Adams *et al.* [STAR Collaboration], Nucl. Phys. A **757**, 102 (2005).

[2] For a recent review, see P. Braun-Munzinger, V. Koch, T. Schafer, and J. Stachel, Phys. Rept. **621**, 76 (2016).

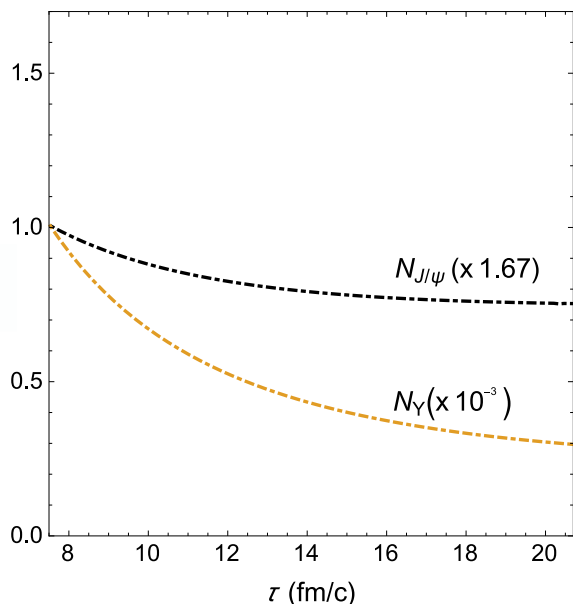


FIG. 8. Top: Time evolution of J/ψ (upper line) and Υ (lower line) abundances as a function of the proper time in central Pb-Pb collisions at the LHC.

- [3] T. Matsui and H. Satz, Phys. Lett. B **178**, 416 (1986).
- [4] For a review, see R. Rapp, Prog. Part. Nucl. Phys. **65**, 209 (2010).
- [5] A. Andronic *et al.*, Eur. Phys. J. C **76**, 107 (2016) and references therein.
- [6] R. L. Thews, M. Schroedter, and J. Rafelski, Phys. Rev. C **63**, 054905 (2001); P. Braun-Munzinger and J. Stachel, Phys. Lett. B **490**, 196 (2000).
- [7] B. B. Abelev *et al.* (Collaboration ALICE), Phys. Lett. B **734**, 314 (2014).
- [8] J. Adam *et al.* (Collaboration ALICE), Phys. Lett. B **766**, 212 (2017).
- [9] W. Zha and Z. Tang, Nucl. Part. Phys. Proc. **289**, 83 (2017).
- [10] X. Du, R. Rapp and M. He, Phys. Rev. C **96**, 054901 (2017).
- [11] A. Andronic, P. Braun-Munzinger, K. Redlich, and J. Stachel, Phys. Lett. B **652**, 259 (2007); M. I. Gorenstein, A. P. Kostyuk, H. Stoecker, and W. Greiner, Phys. Lett. B **509**, 277 (2001).
- [12] Y. Liu *et al.*, Phys. Lett. B **697**, 32 (2011); K. Zhou, N. Xu and P. Zhuang, Nucl. Phys. A **931**, 654 (2014).
- [13] A. Emerick, X. Zhao and R. Rapp, Eur. Phys. J. A **48**, 72 (2012).
- [14] B. Krouppa and M. Strickland, Universe **2**, 16 (2016).
- [15] B. Krouppa, R. Ryblewski, and M. Strickland, Phys. Rev. C **92**, 061901 (2015).
- [16] Z. Hu, N. T. Leonardo, T. Liu and M. Haytmyradov, Int. J. Mod. Phys. A **32**, 1730015 (2017).
- [17] CMS Collab. (S. Chatrchyan *et al.*), Phys. Rev. Lett. **107**, 052302 (2011); Z. Hu, J. Phys. G **38**, 124071 (2011); CMS Collab. (S. Chatrchyan *et al.*), J. High Energy Phys. **05**, 063 (2012).
- [18] L. Adamczyk *et al.* [STAR Collaboration], Phys. Lett. B **735**, 127 (2014); Erratum: [Phys. Lett. B **743**, 537 (2015)].
- [19] V. Khachatryan *et al.* [CMS Collaboration], Eur. Phys. J. C **77**, 252 (2017).
- [20] A. M. Sirunyan *et al.* [CMS Collaboration], arXiv:1805.09215 [hep-ex].
- [21] V. Khachatryan *et al.* [CMS Collaboration], Phys. Lett. B **770**, 357 (2017).
- [22] V. Khachatryan *et al.* [CMS Collaboration], Phys. Lett. B **04**, 031 (2017).
- [23] V. M. Shapoval, P. Braun-Munzinger and Y. M. Sinyukov, Nucl. Phys. A **968**, 391 (2017).
- [24] J. Adam *et al.* [ALICE Collaboration], production at in Pb-Pb collisions Phys. Rev. C **95**, 064606 (2017); B. B. Abelev *et al.* [ALICE Collaboration], Phys. Rev. C **91**, 024609 (2015).
- [25] B. B. Abelev *et al.* (The ALICE Collaboration), Phys. Rev. C **91**, 024609 (2015).
- [26] V. G. Riabov *et al.* (The ALICE Collaboration), J. Phys. Conf. Ser. **798**, 012054 (2017); C. Markert *et al.* (The ALICE Collaboration), J. Phys. Conf. Ser. **878**, 012003 (2017).
- [27] L. M. Abreu, K. P. Khemchandani, A. Martínez Torres, F. S. Navarra and M. Nielsen, Phys. Rev. C **97**, 044902 (2018).
- [28] S. G. Matinyan and B. Müller, Phys. Rev. C **58**, 2994 (1998); A. Bourque and C. Gale, Phys. Rev. C **80**, 015204 (2009); Phys. Rev. C **78**, 035206 (2008); A. Bourque, C. Gale and K. L. Haglin, Phys. Rev. C **70**, 055203 (2004); Z. Lin and C. M. Ko, Phys. Rev. C **62**, 034903 (2000); J. Phys. G **27**, 617 (2001); F. S. Navarra, M. Nielsen and M. R. Robilotta, Phys. Rev. C **64**, 021901(R) (2001); K. L. Haglin and C. Gale, Phys. Rev. C **63**, 065201 (2001); K. L. Haglin, Phys. Rev. C **61**, 031902 (2000); F. Carvalho, F. O. Duraes, F. S. Navarra and M. Nielsen, Phys. Rev. C **72**, 024902 (2005).
- [29] Y. Oh, T. Song and S. H. Lee, Phys. Rev. C **63**, 034901 (2001).
- [30] K. P. Khemchandani, A. Martínez Torres, M. Nielsen and F. S. Navarra, Phys. Rev. D **89**, 014029 (2014).
- [31] F. O. Duraes, H. c. Kim, S. H. Lee, F. S. Navarra and M. Nielsen, Phys. Rev. C **68**, 035208 (2003); F. O. Duraes, S. H. Lee, F. S. Navarra and M. Nielsen, Phys. Lett. B **564**, 97 (2003); F. S. Navarra, M. Nielsen, R. S. Marques de Carvalho and G. Krein, Phys. Lett. B **529**, 87 (2002).
- [32] Z. Lin and C. M. Ko, Phys. Lett. B **503**, 104 (2001).
- [33] H. Nagahiro, L. Roca and E. Oset, Eur. Phys. J. A **36**, 73 (2008).
- [34] A. Martínez Torres, K. P. Khemchandani, F. S. Navarra, M. Nielsen and L. M. Abreu, Phys. Rev. D **90**, 114023 (2014) Erratum: [Phys. Rev. D **93**, 059902 (2016)].
- [35] L. M. Abreu, K. P. Khemchandani, A. Martínez Torres, F. S. Navarra and M. Nielsen, Phys. Lett. B **761**, 303 (2016).
- [36] B. C. Pearce and B. K. Jennings, Nucl. Phys. A **528**, 655 (1991).
- [37] Y. s. Oh, T. s. Song, S. H. Lee and C. Y. Wong, J. Korean Phys. Soc. **43**, 1003 (2003).
- [38] D. Ronchen *et al.*, Eur. Phys. J. A **49**, 44 (2013).
- [39] P. Koch, B. Muller and J. Rafelski, Phys. Rep. **142**, 167 (1986).
- [40] S. Cho *et al.* (ExHIC Collaboration), Phys. Rev. Lett. **106**, 212001 (2011).
- [41] S. Cho and S. H. Lee, Phys. Rev. C **97**, 034908 (2018).
- [42] S. Cho *et al.* (ExHIC Collaboration), Phys. Rev. C **84**,

- 064910 (2011).
- [43] S. Cho *et al.* (ExHIC Collaboration), Prog. Part. Nucl. Phys. **95**, 279 (2017).
- [44] L. W. Chen, C. M. Ko, W. Liu and M. Nielsen, Phys. Rev. C **76**, 014906 (2007).
- [45] S. Cho and S. H. Lee, Phys. Rev. C **88**, 054901 (2013) .